Flow Regimes and Transient Dynamics of Two-Dimensional Stratified Flow over an Isolated Mountain Ridge

YUH-LANG LIN AND TING-AN WANG

Department of Marine, Earth and Atmospheric Sciences, North Carolina State University, Raleigh, North Carolina

(Manuscript received 24 October 1994, in final form 6 July 1995)

ABSTRACT

Four regimes are identified for two-dimensional, unstructured, nonrotating, continuously stratified, hydrostatic, uniform Boussinesq flow over an isolated mountain ridge: (I) flow with neither wave breaking aloft nor upstream blocking ($F \geq 1.12$, where $F = U/Nh$; U and N are upstream basic flow speed and Brunt–Väisälä frequency, respectively; and h is the mountain height), (II) flow with wave breaking aloft in the absence of upstream blocking ($0.9 < F \leq 1.12$), (III) flow with both wave breaking and upstream blocking, but where wave breaking occurs first ($0.6 < F \leq 0.9$), and (IV) flow with both wave breaking and upstream blocking, but where blocking occurs first ($0.3 \leq F \leq 0.6$). In regime I, neither wave breaking nor upstream blocking occurs, but columnar disturbance does exist. The basic flow structure resembles either linear or weakly nonlinear mountain waves. It is found that the columnar disturbance is independent of the wave breaking aloft. In regime II, an internal jump forms at the downstream edge of the wave-breaking region, propagates downstream, and then becomes quasi-stationary. The region of wave breaking also extends downward toward the lee slope. After the internal jump travels farther downstream, a stationary mountain wave becomes established in the vicinity of the mountain above the dividing streamline, which is induced by wave breaking. A high-drag state is predicted in this flow regime. In addition, a vertically propagating hydrostatic gravity wave is generated by the propagating jump and travels with it. Along the lee slope, a strong downslope wind develops. Static and Kelvin–Helmholtz instabilities may occur locally in the region of wave breaking. The critical F for wave breaking is about 1.12, which agrees well with the value 1.18 found by Miles and Huppert. This study also found that the flow responses in this flow regime, as well as in the other regimes, are similar for constant F.

In regime III, the downstream internal jump propagates downstream in the early stage, retrogresses in the direction against the basic flow once blocking occurs, and then becomes quasi-stationary. The retrogression of the downstream jump may be caused by the modification of the upstream boundary conditions. The layer depth of blocked fluid is independent of F and h/a, where a is the mountain half-width. In regime IV, the internal jump quickly becomes stationary over the lee slope once it forms. It is found that the presence of wave breaking aloft is not necessary for upstream blocking to occur. A vertically propagating gravity wave is generated by the upstream reversed flow and travels with it. The speed of the upstream reversed flow is proportional to h/a. The surface drag increases abruptly from regime I to II, while it decreases gradually from regime II (III) to III (IV). The surface drag is a function of h/a and is a minimum for $h/a = 0.05$ for constant F. The average dividing streamline height generated by wave breaking is roughly $0.85\lambda_z$ ($H_dN/U = 5.34$), and the level at which overturning initially occurs is found to be about 4.4 in the high-drag state, where λ_z and H_d are the dimensional hydrostatic vertical wavelength and dividing streamline height, respectively. This indicates that the initial wave overturning occurs at the level of the largest gradient of streamline deflection. It is found that nonlinearity tends to accelerate the upslope flow, decelerate the flow near the mountain peak and top of the leeslope, and accelerate the flow near the internal jump.

1. Introduction

The response of a stably stratified flow over an isolated mountain ridge has been studied extensively in the last four decades (see Queney et al. 1960 and Smith 1979 for reviews). However, some phenomena, such as wave breaking, upstream blocking, generation of severe downslope winds, etc., are still not well understood (see Baines 1987 and Smith 1989a for reviews).

In one-layer hydraulic theory, there exist five flow regimes: (a) supercritical flow with no hydraulic jumps, (b) flow with both upstream and downstream propagating jumps, (c) flow with upstream propagating jump and downstream stationary jump, (d) completely blocked flow, and (e) subcritical flow with no hydraulic jumps (Long 1954, 1972; Houghton and Kasahara 1968). These flow regimes are determined by two parameters, namely, the shallow water Froude number $F_0 = U/\sqrt{gH}$ and the nondimensional mountain height h/H, where U and H are the upstream velocity and fluid depth, respectively. However, the flow parameters in a continuously stratified fluid are different. Three flow parameters for a semi-infinite, continuously stratified

Corresponding author address: Prof. Yuh-Lang Lin, Dept. of Marine, Earth and Atmospheric Sciences, North Carolina State University, Raleigh, NC 27695-8208.

fluid may be defined: U/Nh, h/a, and Na/U (Miles and Huppert 1969), where N, h, and a are, respectively, Brunt–Väisälä frequency, mountain height, and mountain half-width. However, only two of them are independent, since the differential equation governing the flow response is two-dimensional (Laprise and Peltier 1989b). The nondimensional parameter U/Nh (also denoted as F in this study) measures the degree of linearity, h/a measures the steepness of flow streamlines, while Na/U measures the degree of hydrostaticity. Since the numerical model used in this study is Boussinesq and hydrostatic, only one nondimensional parameter is left. In this study we will use the first two parameters (U/Nh and h/a) to construct our regime diagram, although it is well known that the steady-state response for unstructured, continuously stratified, hydrostatic flow over an isolated mountain ridge in the absence of stagnation is controlled solely by the linearity parameter U/Nh (Miles and Huppert 1969).

The flow may become stagnant in essentially two regions: over the lee slope in the interior of the fluid and along the upstream slope of the mountain. Since the strongest part of the hydrostatic wave field occurs directly above the mountain (e.g., see Queney et al. 1960), it is often assumed that stagnation also begins aloft, rather than on the upstream slope (e.g., Smith 1989b). Stagnation over the lee slope is responsible for wavebreaking, overturning, and the transition to a severe downslope wind or high-drag state (Clark and Peltier 1977). Assuming that the upstream flow and Brunt–Väisälä frequency are uniform in the absence of wave overturning aloft, Long (1953, 1955) was able to solve the nonlinear steady-state problem analytically, for stratified flow of finite depth over an isolated mountain ridge. Long's solution advances our understanding of orographically forced flow considerably. However, the constant upstream condition assumed by Long may not necessarily be consistent with the flow established naturally by transients, especially if blocking is involved (Garner 1995). Using results from numerical modeling experiments for a wide range of U/Nh of a stratified flow with finite depth, Lamb (1994) was able to show that wave breaking occurs at amplitudes significantly lower than Long's model predicts.

Extending Long's model to a semi-infinite plane, Miles and Huppert (1969) found that the midlevel stagnation occurs at the critical value $Nh/U = 0.85$ ($F = U/Nh \approx 1.18$) for two-dimensional, uniform, hydrostatic flow over a bell-shaped mountain. Solving a nonhydrostatic version of Long's model using the fully nonlinear lower boundary condition, Laprise and Peltier (1989b) showed that the critical steepening occurs at a height close to 3/4 of hydrostatic wavelength, somewhat downstream of the obstacle's crest. The mountain height required to make the streamlines overturn increases as the mountain width decreases and the flow becomes less hydrostatic. They also found that the celebrated value of Miles and Huppert (1969) is valid only in the limit of very broad obstacles ($Na/U \gg 1$, in the hydrostatic limit). Once wave overturning occurs, local convection may be triggered since the flow in this region is superadiabatic (Laprise and Peltier 1989a). Using a nested numerical model, Scinocca and Peltier (1993, 1994) found that this type of local convection is responsible for triggering the severe downslope wind, through a sequencial development. In the first stage, local convection acts to neutralize the region of overturned isentropes. During the next stage, a large-amplitude stationary disturbance develops above the lee slope of the topography. In time, small-scale secondary Kelvin–Helmholtz (K–H) (shear) instability develops in local regions of enhanced shear associated with flow perturbations caused by the large-amplitude disturbance. In the final stage of development, these modes of Kelvin–Helmholtz instability evolve to larger a spatial scale and come to dominate the flow in the mature windstorm state.

The second possible stagnation region is on the upslope of the mountain and occurs because the oncoming flow at the surface level encounters a reversed pressure gradient force that reduces its speed. Stagnation in two dimensions is responsible for flow recirculation, while stagnation in three dimensions is responsible for flow splitting. Using a nonlinear hydraulic theory, Smith (1985) predicted that low-level blocking will begin at $Nh/U = 0.985 \sim 1$ in the presence of wave breaking. The critical values of Nh/U associated with upstream stagnation for uniform stratified flow past three-dimensional obstacles have been studied numerically by Smith and Gronas (1993) and experimentally by Baines and Smith (1993). For two-dimensional stratified flow over a Gaussian-shaped mountain in a numerical model, Pierrehumbert and Wyman (1985) found that the steady-state flow is well described by Long's model up to the point of wave overturning ($Nh/U < 0.75$; $F > 1.33$). For $Nh/U > 0.75$ ($F < 1.33$), upstream columnar disturbances (e.g., Baines 1987) of finite amplitude are generated, whose amplitude is a function of Nh/U. Upstream blocking occurs near a Gaussian-shaped obstacle for $Nh/U > 1.5$ ($F < 0.67$) and near a bell-shaped obstacle for $Nh/U > 1.75$ ($F < 0.57$), but upstream propagation of this blocked fluid is not observed until $Nh/U \geq 2$ ($F \leq 0.5$). Using a tank experiment, Baines and Hoinka (1985) found that upstream columnar disturbances occur for $Nh/U > 0.5$ ($F < 2$) in a flow over a bell-shaped mountain. This threshold value is independent of obstacle shape and is not dependent on midlevel wave overturning [which is not observed until $Nh/U \geq 1.5$ ($F \leq 0.67$)]. Upstream blocking is observed for $1.3 \leq Nh/U \leq 2.2$, the actual value depending on the obstacle shape. For symmetric obstacles, this value is approximately 2. Wave overturning at midlevels occurs for $Nh/U > 1.5$ ($F < 0.67$). Due to the differences found in these studies, we plan to construct a flow regime diagram using carefully designed numerical experiments for uniform, con-

tinuously stratified, nonrotating, Boussinesq, hydrostatic flow over a bell-shaped mountain in order to gain insight into the flow response. Recent tank experiments reveal that there exists a lower (upper) critical F below which wave breaking does not (does) occur for flow over a three-dimensional obstacle (Castro and Snyder 1993). Therefore, it is also important to investigate the existence of such a critical F for two-dimensional fluid, orographically forced flow.

In studying the dynamics of severe downslope winds, Smith (1985) developed a steady-state nonlinear hydrostatic theory based on Long's equation by assuming a dividing streamline beyond which the fluid is essentially quiescent. Between the dividing streamline and its constant upstream height (H_0), there exists a well-mixed turbulent or wave breaking region. Smith's theory predicts that resonance will occur when the nondimensional critical heights are in the range $(1/2 + 2n)\pi < NH_0/U < (3/2 + 2n)\pi$, depending on the mountain height. This result is different from that predicted by the linear theory of Peltier and Clark (1983), which indicates that resonance will occur when $NH_0/U = (1/2 + n)\pi$, for $n = 0, 1, 2, \cdots$, where H_0 is the height of the wave-induced critical level. The critical heights predicted by Smith's theory agree with numerical simulations using prescribed critical levels performed by several authors (e.g., Durran 1986; Bacmeister and Pierrehumbert 1988). Using tank experiments, Rottman and Smith (1989) found that a severe downslope wind state generally exists for mountain height greater than $0.985U/N$, since the effective mountain height is reduced.

In the numerical simulations of flow over obstacles, numerical smoothing or diffusion is often adopted to avoid the nonlinear aliasing caused by the leapfrog time difference and centered spatial difference schemes. In performing numerical experiments during the course of this study, we have found that the onset of downstream propagation of the internal hydraulic jump tends to be delayed by the presence of numerical smoothing. This is analogous to the finding of Richard et al. (1989), in which surface friction tends to delay the onset of strong surface winds and prevents the downstream propagation of the zone of maximum winds. The sensitivity of the numerical results will be addressed in a separate paper and is important since numerical smoothing has been incorporated in most numerical models. In this study, we keep the cumulative effects of numerical smoothing constant.

The objectives of this study are to (a) document the flow regimes for orographically forced, unstructured (constant N), two-dimensional, nonrotating, stratified, hydrostatic, and Boussinesq fluid flow, (b) investigate the occurrence of wave breaking and upstream blocking as a function of F and h/a, and (c) study the dependency of surface drag, height of the dividing streamline, and time and height of initial wave breaking on F and h/a. Emphasis will be placed on the time evolution of internal jumplike disturbances in flows with low F. The numerical model used to perform the simulations is described in section 2, tested against Long's weakly nonlinear theory, and compared with Peltier and Clark's numerical results (1983). The flow behavior for different flow regimes and the associated transient dynamics is presented in section 3. Concluding remarks are made in section 4.

2. Long's nonlinear theory and the nonlinear numerical model

Long's two-dimensional nonlinear theory for flow over an isolated mountain ridge is presented here to provide guidance for comparisons of the flow fields simulated by the nonlinear numerical model. Both the similarities and differences will be discussed below.

a. Long's nonlinear theory

The vertical displacement governing the steady-state, nonlinear response of two-dimensional, semi-infinite, Boussinesq flow characterized by flow velocity (U) and Brunt–Väisälä frequency (N) in the absence of wave overturning in the interior over a finite-amplitude mountain may be written as (Long 1953)

$$\eta_{xx} + \eta_{zz} + l^2\eta = 0, \tag{1}$$

where $l = N/U$ is the Scorer parameter of the basic flow. Performing a Fourier transform of Eq. (1) yields

$$\hat{\eta}_{zz} + (l^2 - k^2)\hat{\eta} = 0. \tag{2}$$

The nonlinear lower boundary condition for Eq. (1) is given by

$$\eta(x, z) = h(x) \quad \text{at} \quad z = h(x). \tag{3}$$

The general solution for Eq. (2) is simply

$$\hat{\eta} = \hat{\eta}(k, 0)e^{i\lambda z}, \quad \text{for} \quad l > k, \tag{4a}$$

$$\hat{\eta} = \hat{\eta}(k, 0)e^{-mz}, \quad \text{for} \quad k > l, \tag{4b}$$

where

$$\lambda = \sqrt{l^2 - k^2}, \quad m = \sqrt{k^2 - l^2}.$$

Notice that the upper radiation and boundedness conditions have been applied to Eqs. (4a) and (4b), respectively, while the linear lower boundary condition has been applied at $z = 0$, instead of at $z = h(x)$. The vertical displacement in physical space is

$$\eta = \mathrm{Re}\left[\int_0^l \hat{\eta}(k, 0)e^{i\lambda z}e^{ikx}dk + \int_l^\infty \hat{\eta}(k, 0)e^{-mz}e^{ikx}dk\right] \tag{5}$$

and may be obtained numerically by using a fast Fourier transform. Notice that the upward propagation energy requires $\mathrm{sign}(k) = \mathrm{sign}(\lambda)$. The solution to Eq.

(2) using the nonlinear lower boundary condition Eq. (3) can be obtained using an iterative method following Laprise and Peltier (1989b). Notice that in the hydrostatic limit, λ in the first integral is replaced by 1 and that the upper limit of the integration is extended to ∞, while the second integral is dropped. In the following discussion we use the hydrostatic version of the solution.

b. *The nonlinear numerical model*

The North Carolina State University Geophysical Fluid Dynamics Model is based on the two-dimensional nonlinear primitive equations governing orographically forced finite-amplitude perturbations in a uniform, nonrotating, continuously stratified, Boussinesq flow in the terrain-following coordinate $\sigma = z_t(z - z_s)/(z_t - z_s)$, where $z_s(x)$ is the mountain geometry and z_t is the top of the computational domain. The horizontal momentum equation, hydrostatic equation, incompressible continuity equation, and thermodynamic energy equation are taken to be

$$\frac{\partial u}{\partial t} + (U + u)\frac{\partial u}{\partial x} + \dot{\sigma}\frac{\partial u}{\partial \sigma} + \frac{1}{\rho_0}\left[\frac{\partial p}{\partial x} + G\frac{\partial p}{\partial \sigma}\right] + \nu u = D_u, \quad (6)$$

$$\frac{1}{\rho_0}\frac{\partial p}{\partial \sigma} = \frac{g\theta}{H\bar{\theta}}, \quad (7)$$

$$\frac{\partial}{\partial x}\left(\frac{z_t}{H}u\right) + \frac{\partial}{\partial \sigma}\left(\frac{z_t}{H}\dot{\sigma}\right) = 0, \quad (8)$$

$$\frac{\partial \theta}{\partial t} + (U + u)\frac{\partial \theta}{\partial x} + \dot{\sigma}\frac{\partial}{\partial \sigma}(\bar{\theta} + \theta) + \nu\theta = D_\theta, \quad (9)$$

where

$$G = \left(\frac{\partial \sigma}{\partial x}\right)_z = \frac{\sigma - z_T}{z_T - z_s}\frac{\partial z_s}{\partial x}; \quad H = \frac{\partial \sigma}{\partial z} = \frac{z_T}{z_T - z_s}.$$

A first-order closure formulation of the subgrid mixing that depends on the relative strengths of stratification and shear is adopted in this model (Lilly 1962; Durran and Klemp 1982). The subgrid-scale effects are introduced to the calculations through the terms D_u and D_θ:

$$D_u = (K_M A)_x + G(K_M A)_\sigma + H(K_M B)_\sigma;$$

$$D_\theta = [K_H(\theta_x + G\theta_\sigma)]_x + G[K_H(\theta_x + G\theta_\sigma)]_\sigma + (K_H H\theta_\sigma)_\sigma,$$

$$A = u_x + Gu_\sigma - Hw_\sigma; \quad B = Hu_\sigma + w_x + Gw_\sigma,$$

$$K_M = k^2\Delta x\Delta z|\mathrm{def}|\left[\max\left(1 - \frac{K_H}{K_M}\mathrm{Ri}, 0\right)\right]^{1/2}$$

$$\mathrm{Ri} = N_L^2/\mathrm{def}^2, \quad \mathrm{def}^2 = A^2 + B^2,$$

$$N_L^2 = g\frac{\partial}{\partial \sigma}[\ln(\theta + \theta)].$$

In this study we assume that $k = 0.21$ and $K_H/K_M = 3$. Some symbols are explained below, while others have their conventional meanings:

u	perturbation horizontal velocity
$\dot{\sigma}$	sigma vertical velocity
p	perturbation pressure
θ	perturbation potential temperature
U	basic-state horizontal velocity
$\bar{\theta}(\sigma)$	basic-state potential temperature
$\nu(\sigma)$	coefficient of Rayleigh friction and Newtonian cooling
ρ_0	constant reference density
T_0	constant reference temperature
K_H	eddy diffusivity of heat
K_M	eddy diffusivity of momentum
Ri	Richardson number
N_L	local Brunt–Väisälä frequency

In deriving Eq. (6), the hydrostatic equation has been used. The governing equations are discretized and numerically integrated over a two-dimensional grid in (x, σ) space. The horizontal (vertical) derivatives are approximated by fourth- (second) order-centered differences. These schemes are identical to those employed in the Cartesian model employed by Lin and Chun (1991) and Lin et al. (1993). The time derivatives are approximated through the leapfrog scheme, with the exception of the first time step, which is computed by forward differencing. Viscous effects are modeled through the inclusion of Rayleigh friction and Newtonian cooling terms, which for all cases reported in this paper are taken to be zero in the physical domain.

Within the terrain-following coordinate system, the lower boundary condition is $\dot{\sigma} = 0$. The upper radiation boundary condition is approximated by placing an artificial viscous absorbing layer (Klemp and Lilly 1978) on top of the physical domain. In this study we have found that the flow behavior is sensitive to the depth of sponge layer, especially when F is near the regime boundary. This problem will be addressed in a companion paper. After performing a large number of numerical experiments, comparing the results against Long's theoretical solutions, and against the numerical results of other authors, we found that very reliable results can be obtained by using a total vertical domain of 3.4 times the vertical wavelength ($2\pi U/N$), the upper half of which is the sponge layer. The lateral boundary conditions are specified by the Orlanski (1976) radiation condition. A five- (three-) point numerical smoother is applied to every field at every time step to damp $2\Delta x$ ($2\Delta t$) waves. The numerical smoothing coefficient has the value $1/256$. In order to control the cumulative effects of smoothing, the number of applications of the smoother is kept the same for all experiments performed in this study.

The time and horizontal grid intervals used in this study are 5 s and 2 km, respectively. The horizontal domain is 256 km. There are 81 vertical grid points, with the interval depending on the vertical wavelength of the case. In this way, any effects from the upper boundary on the solution in the interior are identical. An idealized bell-shaped mountain ridge is used throughout this study:

$$h(x) = \frac{h_0}{(x/a)^2 + 1}, \qquad (10)$$

where h_0 and a are the mountain height and half-width, respectively. The mountain is introduced impulsively in the initially uniform flow.

To test the numerical model, we perform a simulation and compare the results with Long's nonlinear steady-state solution for a semi-infinite domain. Figure 1 shows the total potential temperature and horizontal wind fields for a hydrostatic flow over the bell-shaped mountain [Eq. (10)] produced by numerical simulation (Figs. 1a and 1b) and predicted by Long's solution (Figs. 1c and 1d) at the nondimensional time $Ut/a = 100.8$. The corresponding dimensional time is about 21.52 h. The mountain height–width aspect ratio is 0.1. The linearity parameter (U/Nh) associated with the basic flow is 1.3 and, therefore, falls into the regime with no wave breaking since this value is larger than the critical value 1.18 predicted by Miles and Huppert (1969). The corresponding dimensional parameters are $h_0 = 1$ km, $a = 10$ km, $U = 13$ m s^{-1}, and $N = 0.01$ s^{-1}. Long's solution is obtained by solving the hydrostatic version of Eq. (5) numerically using the nonlinear lower boundary condition Eq. (3). The upstream phase tilt and development of the hydrostatic mountain wave by Long's theory are well simulated by the numerical model. The slight difference between the result from the numerical model and Long's solution is both numerical and physical. Numerical diffusion may contribute to the formation of smoother isentropes in the numerical model. In addition, the influence of the upper boundary in the numerical model may also contribute to the differences between the numerical and theoretical results, especially for those cases near the regime boundary, such as the present case. The model is less sensitive to the influence of the lateral boundary condition, as compared to the upper boundary condition and total depth of the vertical domain. The influence of the numerical schemes on the physical results will be discussed in a companion paper. The upstream flow can be permanently modified by the passage of an upstream propagating columnar disturbance, which may also be partly responsible for the differences between the numerical and theoretical results. Overall, the numerical model is capable of simulating the basic features of a stably stratified flow forced by an isolated mountain ridge. The solution of Long's nonhydrostatic model (not shown) is almost identical to Long's hydrostatic model (Figs. 1c and 1d) since the hydrostatic parameter (Na/U) for this particular case is 7.69, which is smaller than those associated with all other cases presented in this paper.

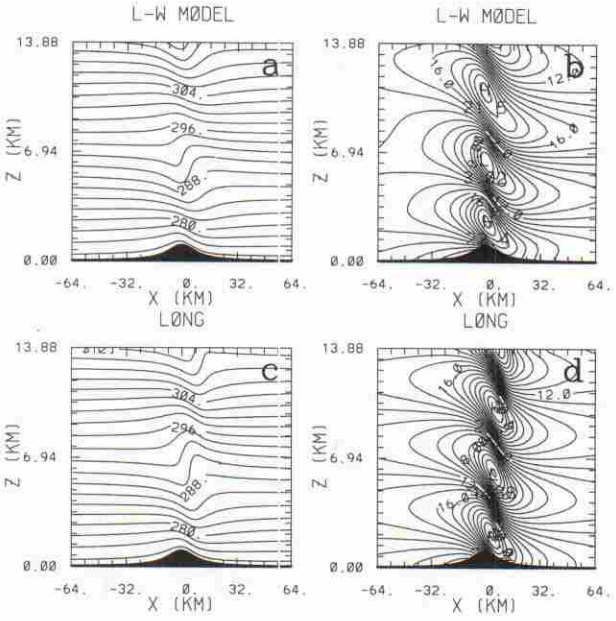

FIG. 1. Potential temperature [(a) and (c)] and total horizontal velocity fields [(b) and (d)] for a two-dimensional, continuously stratified, nonrotating, uniform flow over a bell-shaped mountain at the nondimensional time $Ut/a = 100.8$ [(a) and (b)] and predicted by Long's steady-state hydrostatic solution [(c) and (d)]. The linearity parameter ($F = U/Nh$) and hydrostatic parameter (Na/U) associated with the basic flow are 1.3 and 7.69, respectively. The corresponding dimensional flow parameters are $h = 1$ km, $a = 10$ km, $U = 13$ m s^{-1}, and $N = 0.01$ s^{-1}.

To test the capability of the numerical model to simulate a flow in the regime where $F < 1.18$, in which an overturning layer exists, we run a case identical to Peltier and Clark (1979). Figure 2 shows the total potential temperature fields for a flow over a bell-shaped mountain at the nondimensional times $Ut/a = 8$ and 11.2. The mountain height and width are 500 m and 3 km, respectively. The basic flow velocity and Brunt–Väisälä frequency are 4 m s^{-1} and 0.01 s^{-1}, respectively. The linearity parameter U/Nh and hydrostaticity parameter Na/U are 0.8 and 7.5, respectively. The model's subgrid mixing is deactivated in the present case for direct comparison with Peltier and Clark's results. Peltier and Clark (1979) also used a sponge layer to simulate the upper boundary condition in their nonhydrostatic model. A region of wave overturning develops along the lee slope, and a standing mountain wave develops for $z \geq 2$ km. The wave overturning region extends downward toward the mountain and propagates downstream at later times (not shown). In other words, the results shown are not the true steady state. These results do show, however, that the numerical model is capable of simulating flow with F smaller than

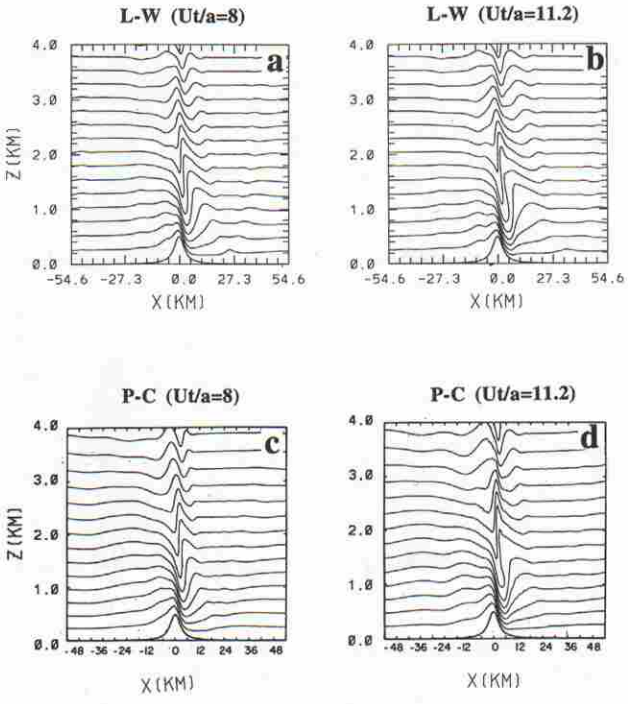

FIG. 2. Potential temperature fields for a two-dimensional, continuously stratified, nonrotating, uniform, hydrostatic flow over a bell-shaped mountain at the nondimensional times $Ut/a = 8$ and 11.2 produced by our hydrostatic model [(a) and (b)] and by Peltier and Clark's (1979) nonhydrostatic model [(c) and (d)]. The linearity parameter (U/Nh) and hydrostatic parameter (Na/U) are 0.8 and 7.5, respectively. The corresponding flow parameters are $U = 4$ m s^{-1}, $N = 0.01$ s^{-1}, and $h_0 = 500$ m.

the critical value. The results shown in Figs. 1 and 2 also suggest that the hydrostatic approximation is reasonable for $Na/U > 7.5$, which is smaller than that used in other studies; that is, $Na/U > 10$ (e.g., Laprise and Peltier 1989b).

3. Flow regimes and transient dynamics

A large number of numerical experiments using the numerical model described in the last section have been performed for stratified, nonrotating, hydrostatic, Boussinesq flow over an isolated two-dimensional bell-shaped mountain ridge. The linearity parameter (U/Nh) ranges from 0.3 to 1.3, while the mountain height–width aspect ratio (h/a) ranges from 0.01 to 0.1. This range of h/a corresponds to mountain height ranging from $h = 100$ m to 1 km for a constant mountain half-width of $a = 10$ km. The nondimensional horizontal model domain ranges from $x = -12.8$ to 12.8, which corresponds to dimensional distances between -128 to 128 km. The nondimensional vertical domain is chosen to be 3.4 times the hydrostatic vertical wavelength ($\lambda_z = 2\pi U/N$). For convenience, the dimensional horizontal and vertical distances are plotted on the figures, unless it is mentioned. However, the flow fields should be regarded as being fully nondimensionalized and can therefore be compared directly with each other. A summary of the flow parameters associated with the numerical experiments performed in this study are presented in Table 1. All flow fields produced by the numerical model are shown at the same nondimensional time, $Ut/a = 50.4$. This allows for direct comparisons between different cases.

Notice that the dimensional simulation time is inversely proportional to h/a for constant F. This implies that the number of applications of the numerical smoother increases for smaller values of h/a as compared to larger h/a if the smoothing coefficient is kept the same. Our numerical experiments indicate that numerical smoothing tends to inhibit the onset time of midlevel wave overturning. Since most of the existing numerical models used to address the two-dimensional orographically flow problem have incorporated some type of numerical smoothing in additional to subgrid mixing, this problem will be addressed in more detail in a separate paper. In this study, we reduce the number of numerical smoothing applications for smaller h/a (cases A, B, and C), so that the cumulative effects of numerical diffusion are the same for all the cases simulated. For example, the dimensional simulation time for case A13 is 10 times longer than that for case D13, since the basic flow velocity is 10 times smaller. Thus, numerical smoothing is applied at every 10 time steps for case A13, rather than applied at every time step for case D13.

Based on the nondimensional times for occurrence of wave breaking and blocking, four separate flow regimes may be identified (Fig. 3): (I) flow with neither wave breaking aloft nor upstream blocking, (II) flow with wave breaking aloft in the absence of upstream blocking, (III) flow with both wave breaking aloft and upstream blocking, but where wave breaking occurs first, and (IV) flow with wave breaking aloft and upstream blocking, but where upstream blocking occurs

TABLE 1. Basic wind speeds (m s^{-1}) used in the numerical experiments. The linearity parameter F is defined as U/Nh. The half-width of the bell-shaped mountain is denoted by a. The other parameters are $N = 0.01$ s^{-1}; $a = 10$ km; $h = 100$, 200, 500; and 1000 m for cases A, B, C, and D, respectively.

Case	F	h/a	A 0.01	B 0.02	C 0.05	D 0.1
13	1.3		1.3	2.6	6.5	13.0
12	1.2		1.2	2.4	6.0	12.0
11	1.1		1.1	2.2	5.5	11.0
10	1.0		1.0	2.0	5.0	10.0
9	0.9		0.9	1.8	4.5	9.0
8	0.8		0.8	1.6	4.0	8.0
7	0.7		0.7	1.4	3.5	7.0
6	0.6		0.6	1.2	3.0	6.0
5	0.5		0.5	1.0	2.5	5.0
4	0.4		0.4	0.8	2.0	4.0
3	0.3		0.3	0.6	1.5	3.0

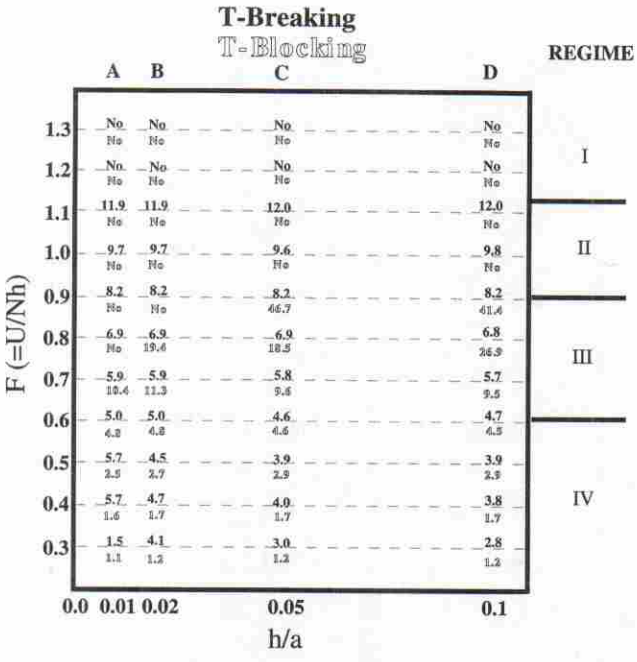

FIG. 3. Regime diagram for two-dimensional, nonrotating, hydrostatic, continuously stratified uniform flow over a bell-shaped mountain ridge. Four flow regimes are identified: (I) flow with neither wave breaking aloft nor upstream blocking, (II) flow with wave breaking aloft and no upstream blocking, (III) flow with both wave breaking and upstream blocking, but where breaking occurs first, and (IV) flow with wave breaking and upstream blocking, but where blocking occurs first. The bold numbers denote the nondimensional times for wave breaking, while the outlined numbers denote the nondimensional times for upstream blocking.

first. The time of upstream blocking is defined as the time at which the total horizontal velocity drops to zero on the windward slope of the obstacle. The potential temperature and total horizontal velocity fields for $h/a = 0.01$, 0.02, 0.05, and 0.1 for $0.3 \leq F \leq 1.3$ at $Ut/a = 50.4$ are shown in Figs. 4 and 5, respectively.

a. Regime I

Two-dimensional, stratified, nonrotating, Boussinesq fluid flow over an isolated mountain ridge in the absence of wave breaking aloft and upstream blocking has been studied extensively using both linear and nonlinear theories and nonlinear numerical models during the last four decades. This type of flow occurs when F is large and the fluid has enough kinetic energy to overcome the potential barrier of the obstacle (e.g., Smith 1979). The linear steady-state solutions have been reviewed by Queney et al. (1960) and Smith (1979). The initial-value problem for a uniform flow over a mountain, which is impulsively set into motion at $t = 0$, has been studied theoretically by Palm (1953).

In this flow regime, the basic flow structure is similar to linear mountain waves except that steeper isentropes form in some weakly nonlinear cases, such as when $F = 1.2$ and 1.3. The numerically simulated vertical wavelengths are very close to those predicted by linear theory and Long's weakly nonlinear theory. The upstream phase tilt and vertical development of the simulated mountain waves, as found in linear mountain waves, are well captured by the model. Therefore, we present only the weakly nonlinear cases with $F = 1.2$ and 1.3. As demonstrated in the last section, the results for case D13 (Fig. 1) compare well with the nonlinear theoretical solutions predicted by Long's model. In this flow regime neither wave overturning nor upstream blocking exists. The numerically simulated flow fields obtained with our hydrostatic-Boussinesq model are almost identical for constant F, even though h/a ranges an order of magnitude from 0.01 to 0.1 (Figs. 4 and 5). This is consistent with the findings of Long (1953, 1955) and Miles and Huppert (1969).

Figure 6 shows the time evolution of the nondimensional total horizontal velocities $(1 + u/U)$ at the surface for cases D13 ($F = 1.3$), D10 ($F = 1.0$), D8 ($F = 0.8$), and D5 ($F = 0.5$). The transient responses of the flow are discussed along with Figs. 7 and 8, which show the time evolution of the total potential temperature and perturbation horizontal velocity fields at the nondimensional times $Ut/a = 12.6$, 25.2, 37.8, and 50.4 for cases in the D category (Table 1). Cases with the same F identified in the flow fields as flows with neither wave breaking nor upstream blocking (Fig. 4) exhibit an almost identical behavior, even though the aspect ratio covers a relatively wide range, $0.01 \leq h/a \leq 0.1$. Two transient waves, which propagate both upstream and downstream, can be detected at early times ($Ut/a \leq 12.6$) from the time evolution of the total horizontal velocity field at the surface (Fig. 6a, denoted by waves 1 and 2) and the vertical cross section of the perturbation horizontal velocity field (Fig. 8). These two waves appear to be generated by the impulsive introduction of the mountain into the uniform flow. The upstream propagating wave travels at a slower speed than the downstream wave due to the advection effect of the basic wind.

The third upstream propagating wave (denoted by wave 3 in Fig. 6a) appears to be more horizontally oriented (case D13 for $Ut/a = 12.6$ and 25.2 in Fig. 8). This wave may be regarded as a *columnar disturbance* (e.g., Pierrehumbert and Wyman 1985; Baines 1987) that permanently alters the upstream temperature and horizontal velocity fields as it passes through the fluid. Pierrehumbert and Wyman suggested that the columnar disturbance is excited by wave breaking above the mountain top. Unlike that described in Pierrehumbert and Wyman (1985), it appears that this disturbance is also associated with the impulsive introduction of the mountain and the use of open upstream boundary condition in this numerical model. This result seems to be consistent with the recent findings of Garner (1995). This abrupt change of the lower surface induces an infinite number of forcing frequencies. This

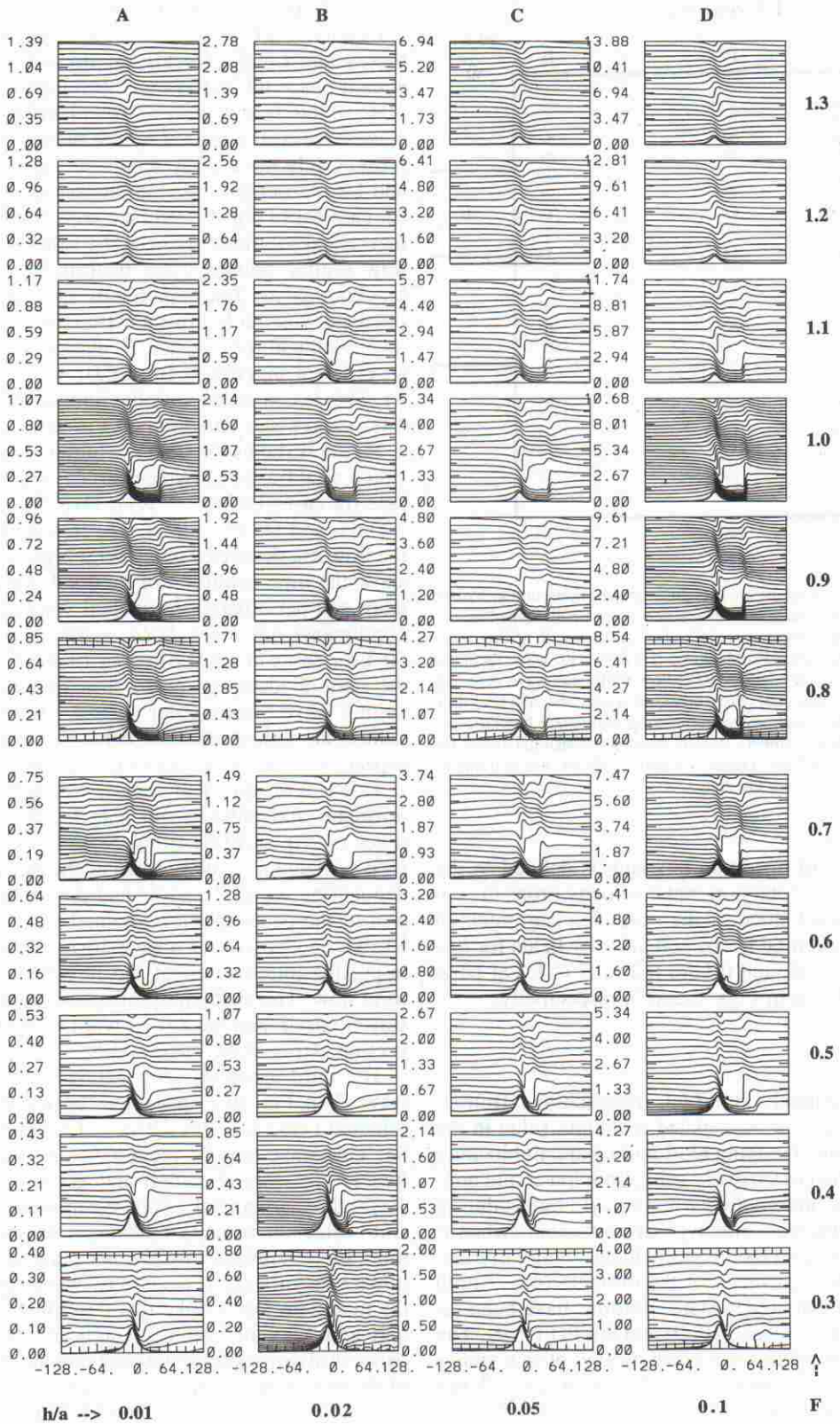

FIG. 4. Potential temperature fields produced by the nonlinear hydrostatic numerical model at $Ut/a = 50.4$ except at $Ut/a = 12.6$ for cases with $F = 0.3$, which correspond to the cases listed in Table 1. Columns A, B, C, and D show cases with $h/a = 0.01$, 0.02, 0.05, and 0.1, respectively. The F ranges from 0.3 (bottom) to 1.3 (top). The entire dimensional computational domain from -128 to $+128$ km is plotted against dimensional height (km). The nondimensional physical domain height is $1.7\lambda_z$.

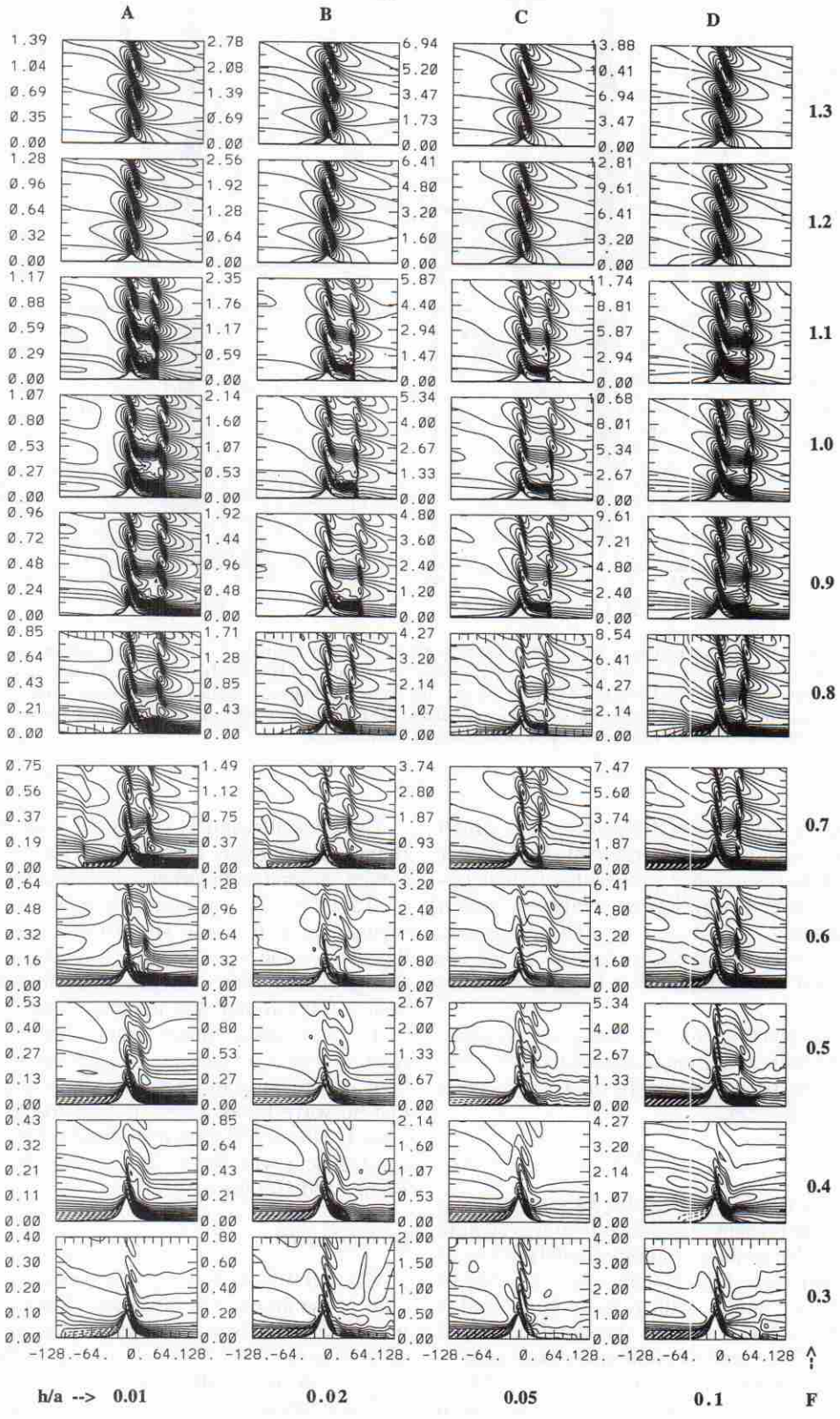

FIG. 5. As in Fig. 4 except for total horizontal velocity fields.

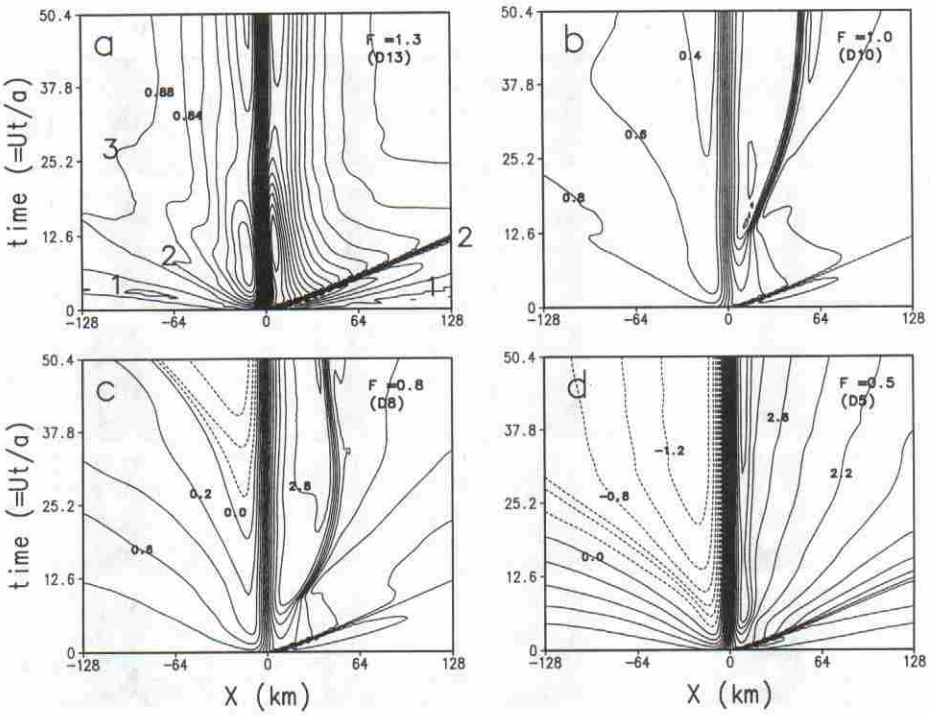

FIG. 6. Time evolution of the nondimensional total horizontal velocities ($1 + u/U$) at the surface for cases: (a) D13 ($F = 1.3$), (b) D10 ($F = 1.0$), (c) D8 ($F = 0.8$), and (d) D5 ($F = 0.5$). The nondimensional contour intervals are 0.04 for (a) and 0.2 for (b)–(d). Some contours are labeled using a smaller font. Transient waves generated by the impulsive introduction of the mountain are denoted as 1, 2, and 3 using a larger font. Wave 3 may be regarded as the columnar disturbance.

wave mode has a much lower frequency (ω), which lies at an angle $\sin^{-1}\omega/N$ to the horizontal (e.g., Turner 1973). When this disturbance propagates farther upstream, the horizontal wavelength increases, which eventually approaches infinity as $t \to \infty$. The asymptotic solution as $t \to \infty$ is that the upstream solutions are periodic in z and independent of x (e.g., Bretherton 1967).

The horizontal phase speed (c_{px}) and group velocity (c_{gx}) associated with a columnar disturbance in a hydrostatic flow can be calculated from the dispersion relationship, which yields

$$c_{px} = c_{gx} = U - N/k_z, \tag{11}$$

where k_z is the vertical wave number of the columnar disturbance. In the present case the vertical wavelength of the columnar disturbance is approximately 6 km, as can be estimated from Fig. 8. This gives a value of -3.45 m s^{-1} for c_{px} and c_{gx} with $U = 13$ m s^{-1} and $N = 0.01$ s^{-1}. This value is close to the simulated speed of -4.95 m s^{-1}. This type of columnar disturbance is also generated in other flow regimes (Fig. 8). However, the columnar disturbance is much weaker than the disturbance associated with upstream blocking in regimes III and IV and, therefore, is more difficult to detect.

The present result is consistent with the finding of Baines and Hoinka (1985), which showed that the upstream columnar disturbances are observed for $Nh/U > 0.5$ ($F < 2.0$) in stratified flow over bell-shaped mountains. Baines and Hoinka also showed that this threshold value is, in general, a function of the mountain geometry. For example, Pierrehumbert and Wyman (1985) found that it requires $Nh/U > 0.75$ ($F < 1.33$) for the columnar disturbance to form in stratified flow over a Gaussian-shaped mountain generated by wave breaking above the lee slope. Our results show that no wave breaking exists over the lee slope in regime I. This is different from their results. However, it is consistent with the tank experiments performed by Baines and Hoinka (1985).

b. Regime II

When $0.9 \leq F \leq 1.12$, there exists wave breaking aloft in the absence of upstream blocking. An internal jump is able to form over the lee slope and propagates downstream in this flow regime (cases D11 and D10, Fig. 7). In this study a jump is defined as the flow response when there exists a region of wave overturning (i.e. $U + u = 0$ aloft) where the isentrope becomes vertical and is able to restore its upstream height level downstream. The flow patterns are still similar for con-

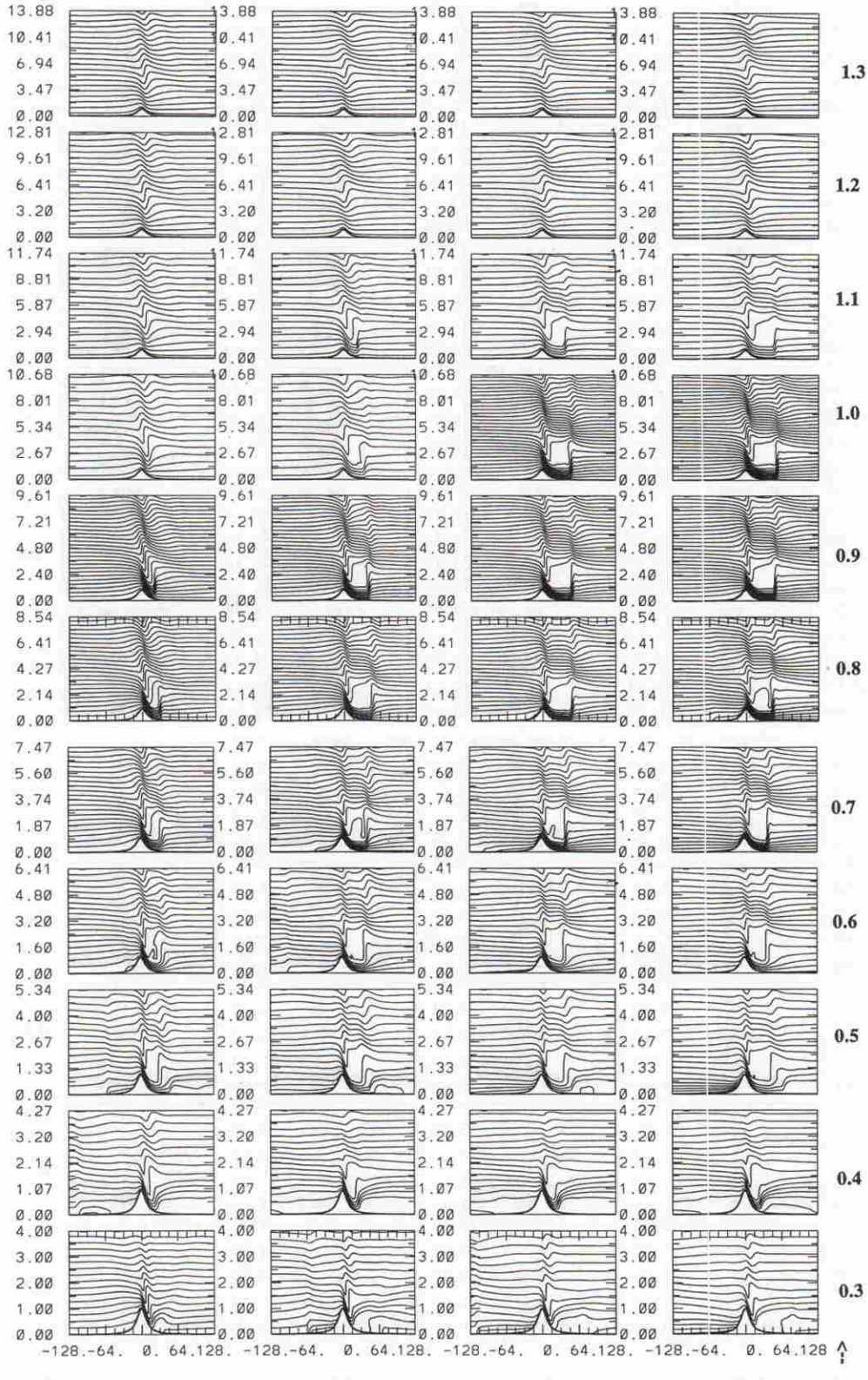

FIG. 7. Time evolution of the potential temperature fields for the cases in category D (Table 1) at Ut/a = 12.6, 25.2, 37.8, and 50.4 (left to right) except those at Ut/a = 3.15, 6.3, 9.45, and 12.6 for cases with F = 0.3.

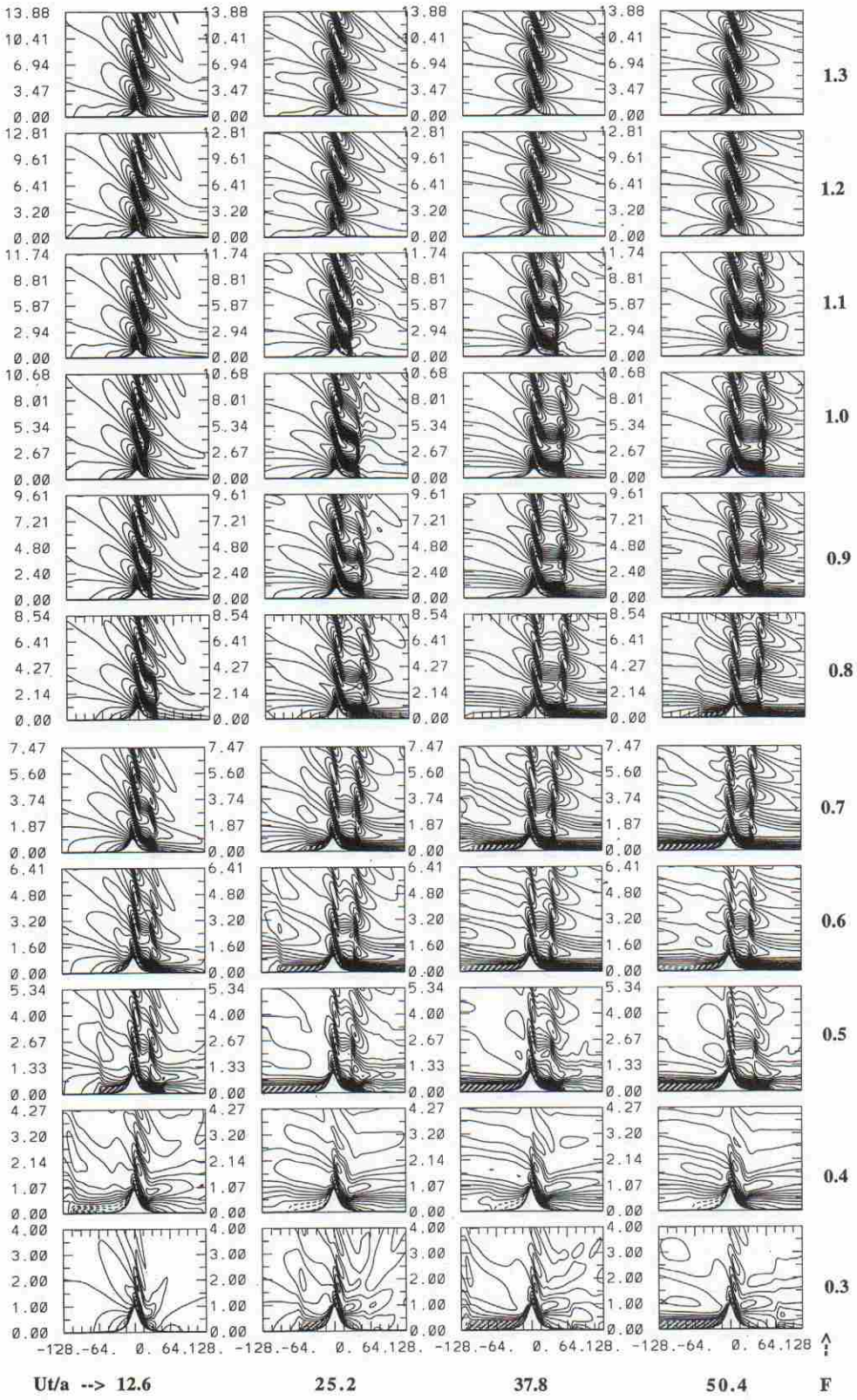

FIG. 8. As in Fig. 7 except for total horizontal velocity fields.

stant F (Fig. 4); that is, they are similar for $0.01 \leq h/a \leq 0.1$. *In this flow regime, no upstream blocking exists.* This is also examined by extending the simulation time (not shown). After the internal jump travels farther downstream, a stationary hydrostatic gravity wave becomes established near the mountain, where structure is similar to linear or weakly nonlinear mountain waves (Fig. 9a). A vertically propagating gravity wave is generated by the internal jump and travels downstream with it (Figs. 5 and 8). This propagating gravity wave may be regarded as analogous to that generated by a propagating density current (Lin and Chun 1991). Along the lee slope, a strong downslope wind develops (Fig. 5), which is evident from the time evolution of the total horizontal wind fields (Figs. 6 and 8).

Similar to regime I, the upstream influence is set up by the upstream propagating columnar disturbance (Fig. 8). When $Ut/a \approx 12.6$ in cases D10 and D11 (Fig. 7), the flow starts to steepen in the layer from 1.5 to 4 km over the lee slope. The gravity wave actually breaks in this layer before $Ut/a = 25.2$. A jumplike disturbance forms at the downstream edge of this wave-breaking region, which is analogous to the hydraulic jump in a shallow water system (Houghton and Kasahara 1968). Notice that unlike conventional hydraulic theory, no upstream propagating jumplike disturbance (bore) is generated, although Pierrehumbert and Wyman (1985) proposed that the columnar disturbance is analogous to the upstream propagating jump in the shallow water system. However, the columnar disturbance in a stratified fluid is significantly weaker than the downstream propagating internal jump. A region of strong upward motion downstream of the lee slope is associated with this jumplike disturbance, which is vertically erect from the surface to a height of about 4 km for case D10 (Fig. 9a). The maximum vertical velocity of this jumplike disturbance at $Ut/a = 50.4$ is about 2 m s^{-1}. In addition to this region of upward motion, there exists another major region of upward motion over the mountain peak, which is associated with the stationary hydrostatic mountain wave. Once the jump forms, it propagates downstream as time proceeds. The propagation speed for case D10 is about 1.0 m s^{-1} during the early stages of the response (Fig. 6b). However, the propagation speed becomes smaller at later times. This downstream jump eventually becomes quasi-stationary (Fig. 6b). After the internal jump propagates away from the mountain, the flow in the vicinity of the mountain reaches a quasi-steady state, and the low-level isentropes exhibit a waterfall-like profile.

The fluid decelerates in the region of wave breaking, which occupies a layer from about 1.5 to 4 km for case D10. This well-mixed region may be classified as a *dead region* (Smith 1985), although the fluid particles above this region are allowed to flow freely in the present numerical model rather than remain stagnant as in Smith's theory. The local Richardson number (N^2/u_z^2) is less (greater) than 0.25 in this wave break-

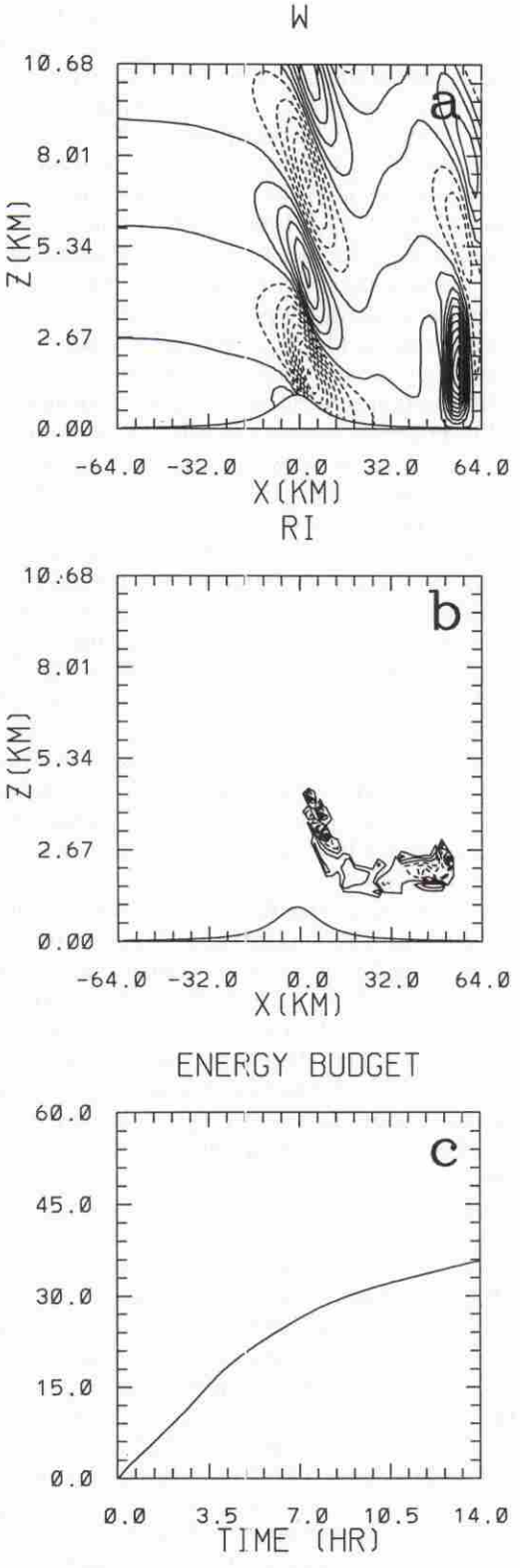

FIG. 9. Case D10: (a) vertical velocity at $Ut/a = 50.4$, (b) Richardson number ($\mathrm{Ri} \leq 0.25$) at $Ut/a = 50.4$, and (c) time evolution of the total perturbation energy. The energy is nondimensionalized by $(1/2)\rho_0 U^2$ times the domain area. Thin-dashed lines denote $u < 0$. The contour intervals for w and Ri are 0.2 m s^{-1} and 0.08, respectively.

ing region (elsewhere) at $Ut/a = 50.4$ (Fig. 9b). This implies that there exist possible static and Kelvin–Helmholtz instabilities in the flow system, which is evident from the increase of total perturbation energy over time (Fig. 9c). The occurrence of Kelvin–Helmholtz instability has also been found by Smith (1991) using a two-layer version of Long's model and by Scinocca and Peltier (1993, 1994) using a nonhydrostatic numerical model. Scinocca and Peltier found that the local convection triggered by wave overturning is responsible for sequentially producing the severe downslope wind, that is, the development of a large-amplitude stationary wave, small-scale Kelvin–Helmholtz instability, and subsequent downstream expansion. The instability primarily remains locally within the region of wave breaking, as shown in Fig. 9b. The isentrope located at approximately 4.9 km (case D10, Fig. 7) may be regarded as the dividing streamline analogous to that predicted by Smith (1985). Below this well-mixed region is a region of strongly accelerated air near the lee slope. This flow acceleration is responsible for producing the strong downslope wind, which reaches a velocity of 28 m s^{-1} near the surface for this case. Notice that this value is about three times the basic flow speed. Above the dividing streamline, an upward propagating internal gravity wave is present over the mountain peak. The response aloft above the flow-induced dividing streamline produced by wave breaking appears to be much less nonlinear than that below the dividing streamline.

Figure 10 summarizes the critical linearity parameter (U/Nh) for wave breaking, as found in the present study in addition to other studies. The critical value is found to be ≈ 1.33 for flow over a Gaussian mountain (Pierrehumbert and Wyman 1985) and 0.67 for flow over a bell-shaped mountain (Baines and Hoinka 1985). The higher value found in the numerical simulations by Pierrehumbert and Wyman may be explained by the stronger nonlinear effect induced by the steeper slope of the Gaussian mountain and possibly some wave reflection from the top boundary since the depth of the sponge layer used in their simulations may not be adequate. The significantly lower value found by Baines and Hoinka's tank experiments may be due to the very high aspect ratio h/a (Smith 1989a) and a shorter simulation time. In addition, the fluid systems in laboratory experiments (e.g., Baines and Hoinka 1985; Castro and Snyder 1993) are nonhydrostatic, which may also contribute to the differences. The present result ($F = 1.12$) compares very well with that ($F = 1.18$) found by Miles and Huppert (1969). The slight difference may be due to the slight change in the upstream condition after the passage of the columnar disturbance and the transient waves generated by the impulsive introduction of the mountain, in addition to the numerical approximations used in the model.

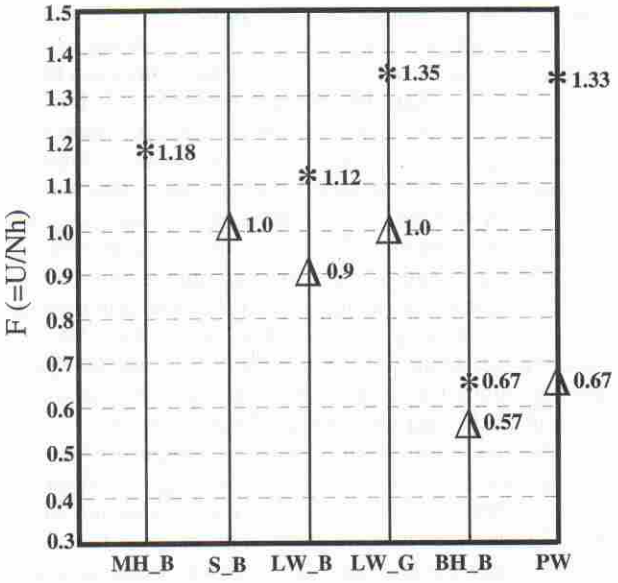

FIG. 10. The critical Fs of wave breaking (*) and upslope blocking (Δ) found in this study (LW_B and LW_G), in Miles and Huppert (MH_B), Smith (S_B), Baines and Hoinka (BH_B), and Pierrehumbert and Wyman (PW_G). Letters B and G represent bell-shaped and Gaussian mountains, respectively.

c. *Regime III*

When $0.6 \leq F \leq 0.9$, there exists both wave breaking aloft and upstream blocking. In this flow regime, the downstream internal jump propagates downstream at early times and then retrogresses in the direction against the basic flow at later times (Figs. 6c, 7, and 8). Eventually, the internal jump becomes quasi-stationary. Unlike flow regime II, upstream blocking occurs. Smith (1985) predicted that low-level blocking will begin at $Nh/U = 0.985 \approx 1$ in the presence of wave breaking over the mountain peak. Our result is consistent with Smith's prediction, although the critical F for wave breaking is smaller ($F \leq 0.9$). Notice that the critical Forude numbers for upstream blocking are found to be 0.57 (Baines and Hoinka 1985) and 0.67 (Pierrehumbert and Wyman 1985). It appears that the difference is partly due to the relatively short simulation times and partly due to different mountain shapes (e.g. Fig. 10). This can be seen by inspecting the blocking time (Fig. 3). Notice that most of the numerical simulations in Pierrehumbert and Wyman are shown at $Ut/a = 25.2$. This will bring the critical F for upstream blocking to be about 0.8, which is much smaller than what it is supposed to be, for bell-shaped mountains in the present case. Similarly, this will happen for Gaussian mountains, which are used by Pierrehumbert and Wyman. The major differences in upstream blocking time for different mountain aspect ratio (h/a) at $F = 0.8$ and 0.9 may be due to truncation errors. Notice that the dimensional simulation times for A cases are 10 time longer than D cases. This is evidenced by the

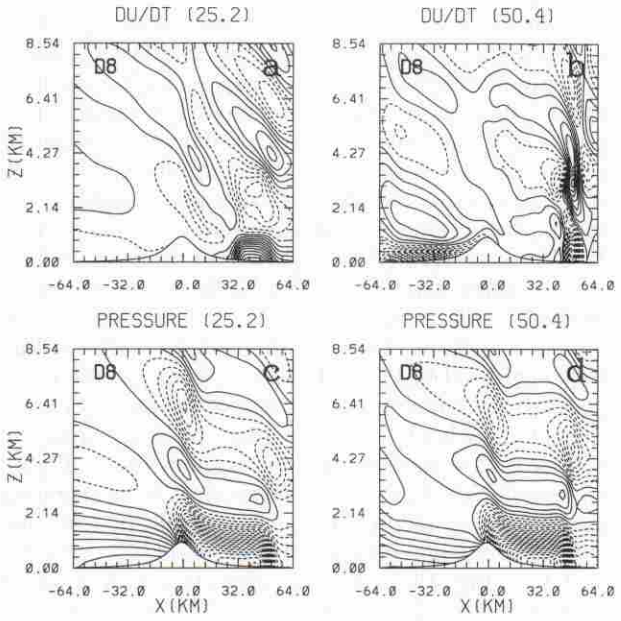

FIG. 11. (a) At $Ut/a = 25.2$, $\partial u/\partial t$, (b) at $Ut/a = 50.4$, $\partial u/\partial t$, (c) at $Ut/a = 25.2$, p, and (d) at $Ut/a = 50.4$, p for case D8 ($F = 0.8$, $h/a = 0.1$).

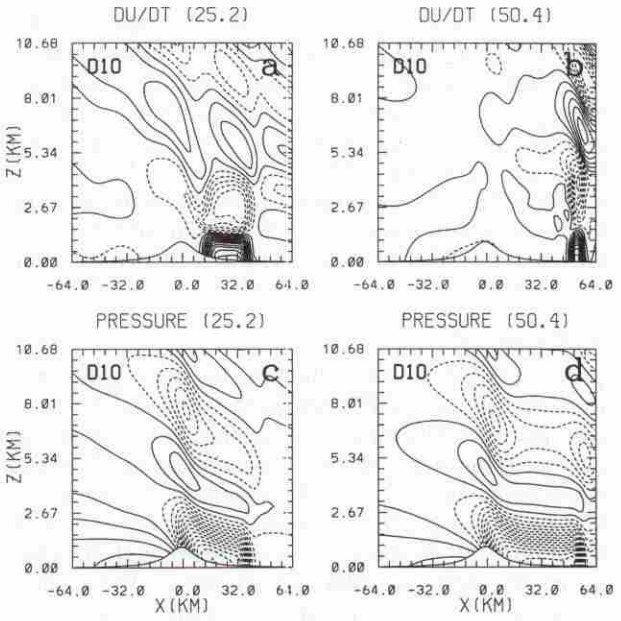

FIG. 12. As in Fig. 11 except for case D10 ($F = 1.0$, $h/a = 0.1$).

fact that major discrepancies occur only at relatively larger blocking times for low mountain aspect ratio, that is, A and B cases.

Once blocking occurs, the downstream propagating jump starts to retrogress, that is, propagate upstream. This can be seen from the time evolution of the total horizontal wind at the surface (Fig. 6c), on the vertical plane (Fig. 7), and in the potential temperature field (Fig. 8). This retrogression appears to be due to the reduction of the effective mountain height when upstream blocking occurs, since the jump travels slower for flows with higher U/Nh (Figs. 7 and 8). We have calculated $\partial u/\partial t$ at $Ut/a = 25.2$ and 50.4, which represents the imbalance between the inertial force, $-(U + u)\partial u/\partial x$, and the pressure gradient force, $-(1/\rho_0)\partial p/\partial x$. The results for case D8 (Figs. 11a and 11b) indicate that the fluid is accelerating over the lee slope behind the jump at $Ut/a = 25.2$ and decelerating near the internal jump at $Ut/a = 50.4$. This deceleration is due to a pressure gradient force that is larger than the inertial force across the internal jump ($-x$ direction) as can be seen from Fig. 11d. Notice that $\partial u/\partial t < 0$ over the upslope is responsible for the layer of deceleration and blocked fluid. This type of retrogression is not present in a flow with no upstream blocking (regime II), in which $\partial u/\partial t$ is always positive (case D10, Figs. 12a and 12b). Similar to regime II, a stationary mountain wave forms in the vicinity of the mountain, and a vertically propagating hydrostatic gravity wave is also generated and propagates along with the internal jump (Figs. 4 and 5). The flow is dynamically unstable in the region of wave breaking.

Figure 5 indicates that the speed of upstream propagating reversed flow is proportional to h/a. In addition, the depth of the blocked fluid layer is a function of F (Fig. 12). The maximum layer depth of the reversed circulation occurs at $x = -32$ km throughout the whole period $0 \leq Ut/a \leq 50.4$. However, there are some inaccuracies in this estimation since the region of recirculation may occur in just a very narrow and shallow region over the upslope side of the topography, such as in case D9 (Figs. 5 and 8). Notice that these simulations are not at all in steady state. For example, Fig. 6c indicates that if one were to integrate somewhat

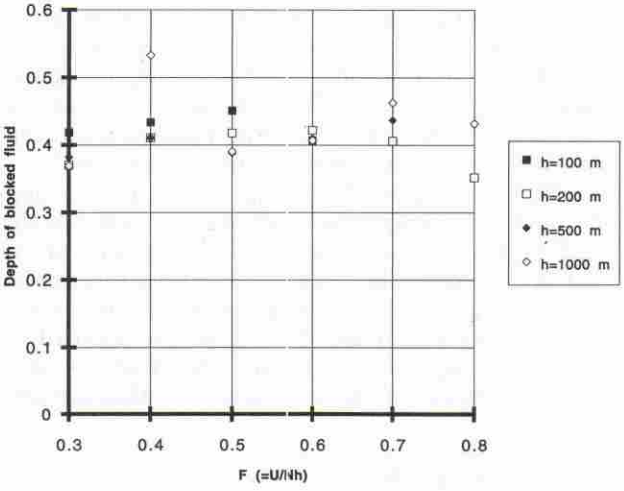

FIG. 13. The depth of blocked fluid vs F for cases A (filled square), B (open square), C (filled diamond), and D (open diamond).

longer, it appears that U would become negative. The nondimensional depth (z_b/H) of the blocked fluid is about 0.425, which is independent of both F and h/a (Fig. 13). The present result is similar to that of Baines (1979), in which he found that $z_b/h = 0.5$. However, he found that blocking occurs only when $F < 0.5$. As mentioned earlier, our numerical simulations show that blocking occurs when $F < 0.9$. In addition, this result differs from Weil et al. (1981) in which they found that $z_b/h \approx 1 - 2F$.

d. Regime IV

When $0.3 \leqslant F \leqslant 0.6$, the flow behavior is different from that in regime III. Although both wave breaking and upstream blocking occur in this flow regime, the upstream blocking occurs earlier than the midlevel wave breaking (Fig. 3). This result is different from that predicted by Smith (1988, 1989b) in which he found that the presence of wave breaking aloft is necessary for upstream blocking to occur. The upslope blocking in this flow regime occurs much earlier than in regime III. This may be due to a more rapid advance of the collapsed density surfaces onto the upstream slope. As mentioned in the introduction, Castro and Snyder (1993) found that there exists a lower critical F below which there is no wave breaking in a stratified flow over a three-dimensional obstacle, in addition to an upper critical F below which wave breaking does occur. The difference between our results and those of Castro and Snyder appear to be related to the fact that our flow is constrained to be two-dimensional, while their flow has full three-dimensionality. In other words, the wave breaking would be delayed or even absent in a three-dimensional flow, since the low-level flow is allowed to go around the mountain (Smith 1988, 1989b).

The internal jump quickly becomes stationary over the lee slope once it forms (Figs. 4, 5, and 6d). This type of jumplike disturbance is analogous to the downstream stationary jump generated in a shallow water system. However, unlike conventional hydraulic theory, there is no upstream propagating jumplike disturbance (bore) generated. Once the upstream blocking occurs, an internal gravity wave is produced and travels upstream with the reversed flow (Fig. 5, case A7). No significant strong wind develops over the lee slope. Therefore, the downstream jump is not evident in the time evolution of the total horizontal velocity at the surface (Fig. 6d). The vertical velocity associated with the jump (not shown) is much weaker than those produced in regimes II and III. Again, the Richardson numbers associated with Kelvin–Helmholtz instability in the region of midlevel wave breaking are less than 0.25.

e. Severe downslope winds

For the flow fields discussed above, some cases exhibit severe downslope winds, such as in regimes II and III. For example, the horizontal wind associated with the downslope wind generated in case D10 is about three times greater (28 m s^{-1}) than the basic-state flow speed (10 m s^{-1}). Figure 14 shows the surface drag produced by the flows for all cases shown in the regime map (Fig. 3), which is nondimensionalized by $(\pi/4)\rho_0 NUh^2$. The surface drag increases abruptly from regime I to regime II. For example, it increases from 1.86 for case D12 ($F = 1.2$) to 4.54 for case D11 ($F = 1.1$) when $h/a = 0.1$. The surface drag decreases gradually from regime II (III) to III (IV) when h/a remains constant. The transition of the surface drag from regime II (III) to III (IV) is rather smooth compared to that from regime I to II. For the present results it is rather difficult to define a high-drag state since the surface drag varies smoothly in Regimes II–IV. Figure 14 also depicts fairly small differences with changing aspect ratio. In addition, the present results indicate that a relatively high drag exists for $Nh/U \geqslant 1.12$ ($F \leqslant 1.12$) (Fig. 14), which is very close to that found by Rottman and Smith (1989) for $Nh/U \geqslant 1$ using tank experiments.

For the response of a basic flow with critical level and constant Brunt–Väisälä frequency forced by a two-dimensional mountain in a numerical model, Bacmeister and Pierrehumbert (1988) found that the high-drag states conform well to the predictions of Smith (1985) based on internal hydraulic analysis and cannot be explained in terms of linear resonance. Smith (1985) defined the dividing streamline induced by wave breaking, to be distinguished from the dividing streamline produced by blocking (e.g., Snyder et al. 1985), as the particular streamline that originates at some level H_d above which only weak mountain waves are present, with the fluid between the two dividing streamlines being well mixed. Nondimensional heights of the divid-

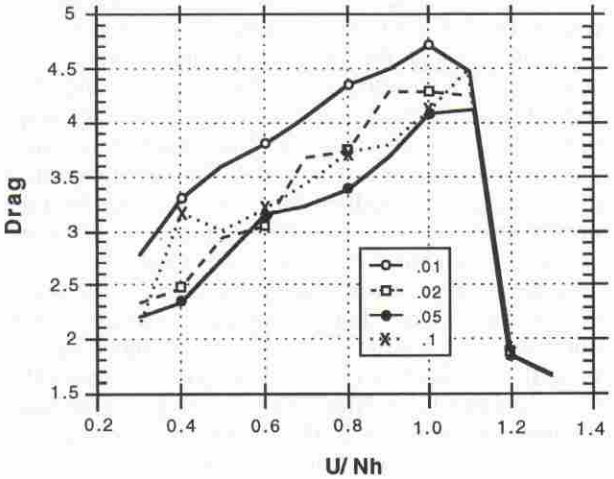

FIG. 14. Surface drags vs F. The surface drags are nondimensionalized by $(\pi/4)\rho_0 NUh^2$. Different curves represent different aspect ratios.

TABLE 2. Nondimensional initial overturning level (H_0N/U).

Case	F	h/a	A 0.01	B 0.02	C 0.05	D 0.1
13	1.3		0.00	0.00	0.00	0.00
12	1.2		0.00	0.00	0.00	0.00
11	1.1		4.27	4.27	4.27	4.27
10	1.0		4.33	4.33	4.33	4.33
9	0.9		4.40	4.40	4.02	4.40
8	0.8		4.52	4.52	4.52	4.08
7	0.7		4.58	4.58	4.58	4.21
6	0.6		4.77	4.77	4.77	4.33
5	0.5		4.71	4.46	4.96	4.46
4	0.4		2.83	4.96	4.77	4.77
3	0.3		0.38	2.64	5.78	5.40

ing streamline (H_dN/U) are estimated for the numerical experiments performed in this study for determining the flow regimes. Unlike in theory (Smith 1985) or in numerical experiments with an imposed zero-wind line in the basic flow (Durran 1986; Durran and Klemp 1987; Bacmeister and Pierrehumbert 1988), it is rather difficult to define a dividing streamline that is produced naturally during the simulated evolution of the flow itself. Therefore, the dividing streamline of wave breaking shown in the present numerical results is defined to be the isentrope that exhibits no jumplike behavior and below which there exists wave breaking and mixing of the fluid. We find that the nondimensional heights of the dividing streamline are almost independent of both F and h/a (Fig. 4). For the cases performed in this study the dividing streamline associated with wave breaking has an average height of $0.85\lambda_z$ ($H_dN/U = 5.34$). Smith (1985, see his Fig. 5) predicts that the nondimensional dividing streamline (H_dN/U) increases almost linearly with Nh/U, whose values fall in the range between $\pi/2$ and $3\pi/2$ for $Nh/U \leqslant 1$. It is difficult to compare the present result with Smith's prediction because most of the cases in this study are for $Nh/U \geqslant 1.12$, while Smith's theory is valid only for $Nh/U \leqslant 1$.

Clark and Peltier (1977) indicated that the initial wave breaking begins near $Nz/U = 3\pi/2$ for a symmetric mountain and suggested that this result would carry over to the final high-drag state. The analysis of Smith (1985) suggested instead that this height is an intrinsic property of the severe wind configuration. Grimshaw and Smyth (1986) showed that the initiation of a high-drag transitional flow begins with linear resonance. According to linear theory, the resonance occurs at $H_0N/U = (1/2 + n)\pi$, $n = 1, 2, 3, \cdots$. In solving a nonhydrostatic version of Long's model with the nonlinear lower boundary condition, Laprise and Peltier (1989b) showed that the critical steepening occurs at a height close to 3/4 of the hydrostatic wavelength ($2\pi U/N$), that is, for $H_0N/U = 3\pi/2$. To investigate this for a wider range of flow parameters, we calculate the initial nondimensional overturning level (H_0N/U) for all the cases shown in Fig. 3. The overturning level is defined to be the height at which the total horizontal wind becomes negative. The results indicate that the overturning level is about 4.4 (Table 2) in regimes II–IV, which is slightly lower than that predicted ($3\pi/2$) by linear resonance theories (Clark and Peltier 1984; Grimshaw and Smyth 1986) and Long's nonlinear model (Laprise and Peltier 1989b). Thus, the initial wave overturning occurs at the level of the largest gradient of streamline deflection. However, as discussed earlier, nonlinearity and Kelvin–Helmholtz instability play essential roles in developing the internal jump and severe downslope wind at later stages.

To investigate the importance of nonlinearity in the development of the internal jump and severe downslope wind, we perform a corresponding linear simulation for case D10. The results at $Ut/a = 25.2$ are shown in Fig. 15. Comparing the potential temperature and total horizontal velocity fields between these two

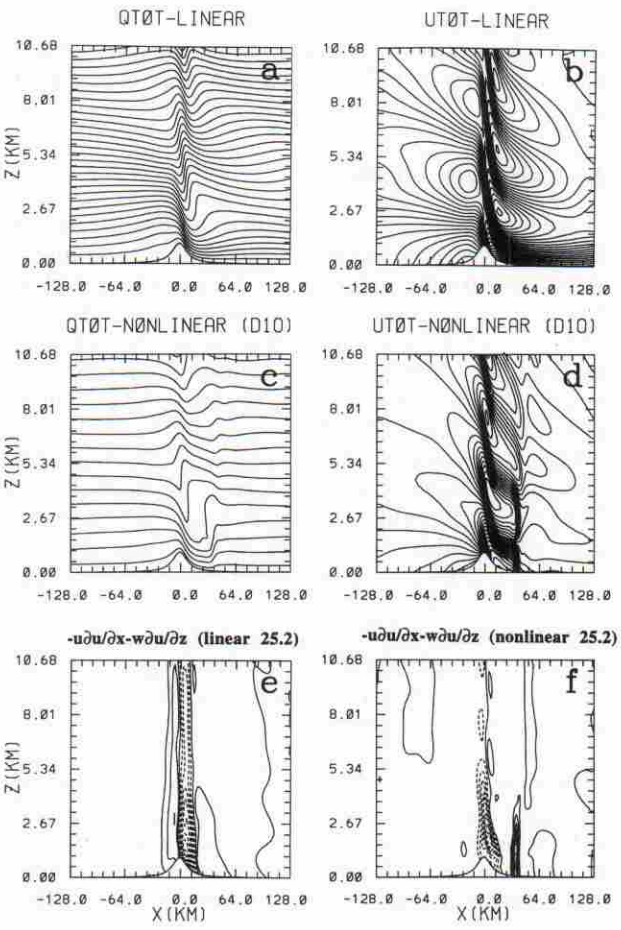

FIG. 15. (a) Potential temperature and (b) total horizontal velocity fields for a corresponding linear simulation of case D10 at $Ut/a = 25.2$. (c) and (d) are similar to (a) and (b) except for the nonlinear case. The summation of the nonlinear terms, $-u\partial u/\partial x - w\partial u/\partial z$, from the linear and nonlinear simulations are shown in (e) and (f), respectively.

cases, we find that in the absence of nonlinear effects (Figs. 15a–d) the internal jump is not able to develop as far downstream as that for a nonlinear flow. It is clear that nonlinearity will help steepen the wave. Notice that the individual nonlinear terms, $-u\partial u/\partial x$ and $-w\partial u/\partial z$, do exhibit vertical wave structure (not shown), but not their summation, since u and w fields are out of phase by a half-wavelength. However, nonlinearity tends to accelerate the upslope flow, decelerate the flow near the mountain top and along the upper part of the leeslope, and accelerate the flow near the internal jump (Fig. 15d). Thus, the upstream blocking produced in the linear flow (Fig. 15b) is diminished for nonlinear flow (Fig. 15d). As shown by Scinocca and Peltier (1993) using a nested grid nonlinear model, the spatially growing modes of the K–H instability are responsible for the strong quasi-periodic surface gusts observed by Neiman et al. (1988). However, the analysis of nonlinear terms in this study indicates that they play an important role in accelerating the internal jump downstream in early times (Figs. 15e and 15f). Notice that the downstream acceleration due to nonlinearity is located farther downstream at later times (not shown), which is almost balanced by the pressure gradient force.

4. Concluding remarks

A large number of numerical experiments are performed for a semi-infinite, unstructured, two-dimensional, hydrostatic, stratified fluid flow over an isolated bell-shaped mountain in order to document the flow regimes and to investigate the occurrence of wave breaking and flow blocking based on the linearity parameter ($F = U/Nh$) and the mountain height–width aspect ratio (h/a). The ranges of F and h/a vary from 0.3 to 1.3 and from 0.01 to 0.1, respectively. It is found that the hydrostatic approximation is reasonable for $Na/U > 0.75$. Four flow regimes are identified: (a) flow with neither wave breaking aloft nor upstream blocking (regime I), (b) flow with wave breaking aloft in the absence of upstream blocking (regime II), (c) flow with both wave breaking and upstream blocking, but where wave breaking occurs first (regime III), and (d) flow with both wave breaking and upstream blocking, but where upstream blocking occurs first (regime IV).

In regime I ($F > 1.12$) neither wave breaking nor upstream blocking exists. In this flow regime the basic flow structure is similar to linear or weak nonlinear mountain waves. The flow responses are independent of h/a, in agreement with that found by Miles and Huppert (1969), and compare well with Long's semi-infinite nonlinear solutions. The stationary mountain wave tilts upstream and has a vertical wavelength close to that predicted by linear theory. Several transient waves form and propagate upstream, which appear to be generated by the impulsive introduction of the mountain into the uniform basic flow. One of these waves propagates upstream at a much slower speed and has a relatively large horizontal wavelength, and is defined as a columnar disturbance. This columner disturbance is much weaker in other flow regimes, compared with the amplitude of the jumplike disturbances. Unlike Pierrehumbert and Wyman (1985), the present results indicate that the occurrence of the columnar disturbance is independent of the midlevel wave breaking.

When $0.9 \leqslant F \leqslant 1.12$ (regime II), wave breaking occurs aloft in the absence of upstream blocking. The region of wave breaking extends downward toward the lee slope at later times. An internal jump forms at the downstream edge of the wave breaking region and propagates downstream in this flow regime. The jump propagates downstream at a faster speed in the early stage of the flow response and then becomes quasi-stationary at later times. After the internal jump travels farther downstream, a stationary mountain wave becomes established above the dividing streamline induced by wave breaking, which exhibits characteristics of linear or weakly nonlinear mountain waves. A high-drag state is observed to exist in this flow regime. The surface drag increases abruptly from regimes I to II. In addition, a vertically propagating gravity wave is generated by the internal jump and travels downstream with it. Along the lee slope, a strong downslope wind develops. In the region above wave breaking, the Richardson number is less than 0.25. The total perturbation energy increases almost linearly with time, which indicates that the Kelvin–Helmholtz instability remains locally within the region of wave breaking. The numerical simulations over long times indicate that the critical F, which separates the regimes of flow with neither wave breaking nor upstream blocking and flow with midlevel wave breaking over the lee slope, is about 1.12. This critical F for wave breaking is very close to the value of 1.18 ($Nh/U = 0.85$) found by Miles and Huppert (1969) but is different from the value of 0.67 found by the tank experiments of Baines and Hoinka (1985). The slight difference between our results and those of Miles and Huppert may be due to the permanent modification of the upstream condition after the passage of transient waves generated by the impulsive introduction of the mountain and the approximations inherent in the numerical model. We also find that the flow responses in this regime, as well as in the other regimes, are similar when h/a varies and F is held constant.

When $0.6 \leqslant F \leqslant 0.9$ (regime III), there exists both wave breaking aloft and upstream blocking, but where the wave breaking occurs first. In this flow regime, the internal jump propagates downstream during the early stages of the flow response and then retrogresses in a direction against the basic flow. Eventually, the jump becomes quasi-stationary. The critical value of $F = 0.9$ for the onset of low-level blocking is smaller than the value (0.985) found by Smith (1985) and is larger than

that found by Baines and Hoinka (1985) and Pierrehumbert and Wyman (1985). It appears that a relatively short simulation time yields a lower critical F. The retrogression of the downstream jump is explained by the reduction in the effective mountain height once blocking occurs, since the jump propagates at a slower speed for flow with a higher F. This is shown by the imbalance between the inertial and the pressure gradient force in the vicinity of the jump. Similar to regime II, a stationary mountain wave forms above the dividing streamline induced by wave breaking. A vertically propagating hydrostatic gravity wave is also generated by the propagating internal jump. In addition, the flow is dynamically unstable in the region of wave breaking. The depth (z_b/h) of the blocked fluid layer is about 0.425 and is independent of F and h/a. This result is similar to that of Baines (1979), for which he found that $z_b/h = 0.5$. Blocking occurs only when $F < 0.5$ for his cases. This result differs from Weil et al. (1981) in which they found that $z_b/h \approx 1 - 2F$. The speed of the reversed flow is proportional to h/a.

When $0.3 \leq F \leq 0.6$ (regime IV), upstream blocking occurs earlier than the midlevel wave breaking. This result is different from that predicted by Smith (1988, 1989b), in which he found that the presence of wave breaking aloft is necessary for upstream blocking to occur. The upstream blocking in this flow regime occurs much earlier than that in regime III. This may be due to a more rapid advance of the collapsed density surfaces onto the upstream slope. In studying flow over a three-dimensional obstacle, Castro and Snyder (1993) found that there exists a lower critical F below which there is no wave breaking, in addition to an upper critical F under which wave breaking occurs. The existence of wave breaking in our results may be due to the assumption of two-dimensionality. In this flow regime, the internal jump quickly becomes stationary over the lee slope once it forms. An internal gravity wave is generated by the reversed flow and travels upstream with it. This type of jumplike disturbance is analogous to the downstream stationary jump generated in a shallow water system. However, no upstream propagating jump forms. The Richardson numbers in the region of wave breaking are less than 0.25. Notice that the detection of wave breaking time at the regime boundary III–IV may be improved by increasing the model resolution. However, the decrease of the upstream blocking time is still faster than that of the wave-breaking time for cases with constant h/a (Fig. 3).

For the flow fields presented in this study, some cases exhibit severe downslope winds, such as those flows in regimes II and III. The transition from regime II (III) to III (IV) is rather smooth, while it is abrupt from regime I to II. The surface drag varies slightly with h/a when F is held constant. The dividing streamline associated with wave breaking has an average height of $0.85\lambda_z$ ($H_dN/U = 5.34$). This value is slightly higher than that ($3\pi/2$) predicted by Clark and Peltier (1984) from numerical experiments and is also different from that predicted by Smith's theory (1985) in which the nondimensional dividing streamline increases almost linearly with Nh/U and falls in the range of $\pi/2$ and $3\pi/2$ for $Nh/U \leq 1$. It is difficult to compare the present result with Smith's theory because most of the cases presented in this study are for $Nh/U \geq 1.12$, while Smith's theory is valid only for $Nh/U \leq 1$. The initial overturning level (H_0N/U) is found to be about 4.4 in the high-drag state, which indicates that the initial wave overturning occurs at the level of the largest linear wave disturbance. It is found that nonlinearity tends to accelerate the upslope flow, decelerate the flow near the mountain top and along the upper part of the leeslope, and accelerate the flow near the internal jump.

In performing the numerical experiments, we have found that the model results are sensitive to some numerical settings—such as the numerical diffusion coefficients, height of the physical domain, depth of the sponge layer that approximates the upper radiation condition, etc.—when F is near the critical value. In particular, the impact of the upstream open boundary condition on the flow regimes deserve further study. The sensitivity of the numerically simulated results will be investigated in a companion paper. In addition, this type of study should be extended to a structured (layered) atmosphere and a shear flow, since observations indicate that strong downslope winds tend to occur when the atmosphere has a multilayer structure (e.g., Klemp and Lilly 1975). The role of the wave-induced critical level associated with wave breaking in affecting the flow regimes should also be studied. A nonhydrostatic model may be needed for investigating the responses of flow over a steep mountain and also the detailed structures of hydraulic jumps and transient eddies, which may have a scale much smaller than the mountain width.

Acknowledgments. This work is supported by the NSF Grant ATM-9224595. Discussions with Drs. R. B. Smith, Dale Durran, R. Rotunno, W. H. Snyder, and G. S. Janowitz are highly appreciated. Comments by Dr. R. Laprise and anonymous reviewers have significantly improved the quality of the paper. The authors also wishes to thank Dr. R. P. Weglarz for proofreading the manuscript and helping to develop the NCSU/GFDM. Part of the computations were performed on the CRAY Y-MP at the North Carolina Supercomputing Center and on the FOAM[v] workstations at NCSU, which are funded by IBM.

REFERENCES

Bacmeister, J. T., and R. T. Pierrehumbert, 1988: On high-drag states of nonlinear stratified flow over an obstacle. *J. Atmos. Sci.*, **45**, 63–80.

Baines, P. G., 1979: Observations of stratified flow past three-dimensional barriers. *J. Geophys. Res.*, **84**, 7834–7838.

——, 1987: Upstream blocking and airflow over mountains. *Annu. Rev. Fluid Mech.*, **19,** 75–97.
——, and K. P. Hoinka, 1985: Stratified flow over two-dimensional topography in fluid of infinite depth: A laboratory simulation. *J. Atmos. Sci.*, **42,** 1614–1630.
——, and R. B. Smith, 1993: Upstream stagnation points in stratified flow past obstacles. *Dyn. Atmos. Oceans,* **18,** 105–113.
Bretherton, F. P., 1967: The time-dependent motion due to a cylinder moving in an unbounded rotating or stratified fluid. *J. Fluid Mech.*, **28,** 545–570.
Castro, I. P., and W. H. Snyder, 1993: Experiments on wave breaking in stratified flow over obstacles. *J. Fluid Mech.*, **255,** 195–211.
Clark, T. L., and W. R. Peltier, 1977: On the evolution and stability of finite-amplitude mountain waves. *J. Atmos. Sci.*, **34,** 1715–1730.
——, and ——, 1984: Critical level reflection and the resonant growth of nonlinear mountain waves. *J. Atmos. Sci.*, **41,** 3122–3134.
Durran, D. R., 1986: Another look at downslope windstorms. Part I: On the development of analogs to supercritical flow in an infinitely deep, continuously stratified fluid. *J. Atmos. Sci.*, **43,** 2527–2543.
——, and J. B. Klemp, 1982: The effects of moisture on trapped mountain lee waves. *J. Atmos. Sci.*, **39,** 2490–2506.
——, and ——, 1987: Another look at downslope winds. Part II: Nonlinear amplification beneath wave-overturning layers. *J. Atmos. Sci.*, **44,** 3402–3412.
Garner, S. T., 1995: Permanent and transient upstream effects in nonlinear stratified flow over a ridge. *J. Atmos. Sci.*, **52,** 227–246.
Grimshaw, R. H., and N. Smyth, 1986: Resonant flow of a stratified fluid over topography. *J. Fluid Mech.*, **169,** 429–464.
Houghton, D. D., and A. Kasahara, 1968: Nonlinear shallow fluid flow over an isolated ridge. *Commun. Pure Appl. Math.*, **21,** 1–23.
Klemp, J. B., and D. K. Lilly, 1975: The dynamics of wave-induced downslope winds. *J. Atmos. Sci.*, **32,** 320–339.
——, and ——, 1978: Numerical simulation of hydrostatic mountain waves. *J. Atmos. Sci.*, **35,** 78–108.
Lamb, K. G., 1994: Numerical simulations of stratified inviscid flow over a smooth obstacle. *J. Fluid. Mech.*, **260,** 1–22.
Laprise, R., and W. R. Peltier, 1989a: The linear stability of nonlinear mountain waves. *J. Atmos. Sci.*, **46,** 545–564.
——, and ——, 1989b: On the structural characteristics of steady finite-amplitude mountain waves over bell-shaped topography. *J. Atmos. Sci.*, **46,** 586–595.
Lilly, D. K., 1962: On the numerical simulation of buoyant convection. *Tellus,* **14,** 148–172.
Lin, Y.-L., and H.-Y. Chun, 1991: Effects of diabatic cooling in a shear flow with a critical level. *J. Atmos. Sci.*, **48,** 2476–2491.
——, T.-A. Wang, and R. P. Weglarz, 1993: Interactions between gravity waves and cold air outflows in a stably stratified uniform flow. *J. Atmos. Sci.*, **50,** 3790–3816.
Long, R. R., 1953: Some aspects of stratified fluids. I. A theoretical investigation. *Tellus,* **5,** 42–58.
——, 1954: Some aspects of the flow of stratified fluids. II. Experiments with a two fluid system. *Tellus,* **6,** 97–115.
——, 1955: Some aspects of the flow of stratified fluids. III. Continuous density gradients. *Tellus,* **7,** 341–357.
——, 1972: Finite amplitude disturbances in the flow of inviscid, rotating and stratified fluids over obstacles. *Annu. Rev. Fluid Mech.*, **4,** 69–92.
Miles, J. W., and H. E. Huppert, 1969: Lee waves in a stratified flow. Part 4: Perturbation approximations. *J. Fluid Mech.*, **35,** 497–525.
Neiman, P. J., R. M. Hardesty, M. A. Shapiro, and R. E. Cupp, 1988: Dopplar Lidar observations of a downslope windstorm. *Mon. Wea. Rev.*, **116,** 2265–2275.
Orlanski, I., 1976: A simple boundary condition for unbounded hyperbolic flow. *J. Comput. Phys.*, **21,** 251–269.
Palm, E., 1953: On the formation of surface waves in a fluid flowing over a corrugated bed and on the development of mountain waves. *Astrophys. Norv.*, **5,** 95–129.
Peltier, W. R., and T. L. Clark, 1979: The evolution and stability of finite-amplitude mountain waves. Part II: Surface wave drag and severe downslope winds. *J. Atmos. Sci.*, **36,** 1498–1529.
——, and ——, 1983: Nonlinear mountain waves in two and three spatial dimensions. *Quart. J. Roy. Meteor. Soc.*, **109,** 527–548.
Pierrehumbert, R. T., and B. Wyman, 1985: Upstream effects of mesoscale mountains. *J. Atmos. Sci.*, **42,** 977–1003.
Queney, P., G. A. Corby, N. Gerbier, H. Koschmieder, and J. Zierep, 1960: The airflow over mountains. WMO Tech. Note 34, 135 pp.
Richard, E., P. Mascart, and E. C. Nickerson, 1989: The role of surface friction in downslope windstorms. *J. Appl. Meteor.*, **28,** 241–251.
Rottman, J. W., and R. B. Smith, 1989: A laboratory model of severe downslope winds. *Tellus,* **41A,** 401–415.
Scinocca, J. F., and W. R. Peltier, 1993: The instability of Long's stationary solution and the evolution toward severe downslope windstorm flow. Part I: Nested grid numerical simulations. *J. Atmos. Sci.*, **50,** 2245–2263.
——, and ——, 1994: The instability of Long's stationary solution and the evolution toward severe downslope windstorm flow. Part II: The application of finite-amplitude local wave-activity flow diagnostics. *J. Atmos. Sci.*, **51,** 623–653.
Smith, R. B., 1979: The influence of mountains on the atmosphere. *Adv. Geophys.*, **21,** 87–230.
——, 1985: On severe downslope winds. *J. Atmos. Sci.*, **42,** 2597–2603.
——, 1988: Linear theory of stratified flow past an isolated mountains in isosteric coordinates. *J. Atmos. Sci.*, **45,** 3889–3896.
——, 1989a: Hydrostatic airflow over mountains. *Advances in Geophysics,* Vol. 31, Academic Press, 1–41.
——, 1989b: Mountain-induced stagnation points in hydrostatic flow. *Tellus,* **41A,** 270–274.
——, 1991: Kelvin–Helmholtz instability in severe downslope wind flow. *J. Atmos. Sci.*, **48,** 1319–1324.
——, and S. Gronas, 1993: Stagnation points and bifurcation in 3-D mountain airflow. *Tellus,* **45A,** 28–43.
Snyder, W. H., R. S. Thompson, R. E. Eskridge, and R. E. Lawson, 1985: The structure of strongly stratified flow over hills: Dividing-streamline concept. *J. Fluid Mech.*, **152,** 249–288.
Turner, J. S., 1973: *Buoyancy Effects in Fluids.* Cambridge University Press, 368 pp.
Weil, J. C., S. C. Traugott, and D. K. Wong, 1981: Stack plume interaction and flow characteristics for a notched ridge. Rep. PPRP-61, Maryland Power Plant Siting Program, Martin Marietta Corp., 92 pp.